Journal of Materials Chemistry A

Accepted Manuscript

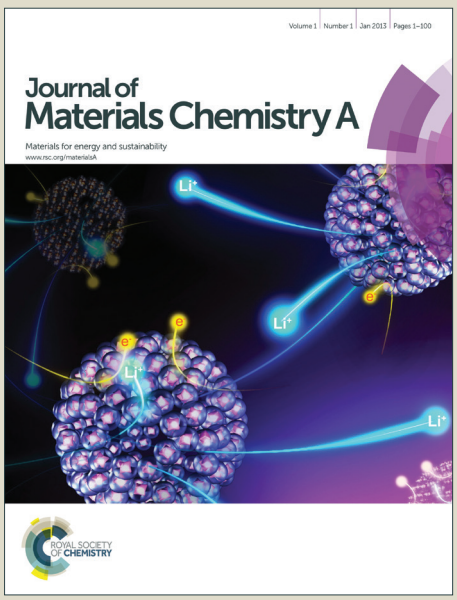

ROYAL SOCIETY OF CHEMISTRY

www.rsc.org/materialsA

In-situ dilatometric and impedance spectroscopic study of core-shell like structures: Insights into the exceptional catalytic activity of nanocrystalline Cu-doped CeO_2

[1,2]Philippe Knauth,[1]Howard Saltsburg, [1]Johanna Engel, [1]Harry L. Tuller

[1] Department of Materials Science and Engineering, MIT, Cambridge, MA 02139, USA

[2]Aix-Marseille University, CNRS, MADIREL (UMR 7246), 13397 Marseille, France

Abstract: Cu-doped CeO_2 (8 mol% Cu) nanoparticles were investigated by combined *in situ* dilatometry and impedance spectroscopy as a means of exploring the impact of temperature and pO_2 driven dopant redistribution and phase separation on both thermo-mechanical and electrical properties of the CuO_x-CeO_2 system. Dilatometry was used to track the thermal expansion of the CeO_2 nanoparticles as well as the reduction of segregated copper oxide into metallic copper when exposed to reducing conditions. The electrical properties of the nanoparticle array, extracted from impedance spectroscopy studies, point to proton conduction at low temperatures, with a transition to n-type electronic conductivity of CeO_2 at higher temperatures. After segregation of percolating interfacial layers, induced by exposure to reducing atmosphere, the electrical properties become dominated by p-type Cu_2O at intermediate pO_2 and metallic copper at low pO_2. The temperature and pO_2 dependent electrical properties of both the Cu_2O shell and the underlying ceria core were examined in light of defect chemical models. Based on these models, the standard formation enthalpy of copper vacancies and holes in Cu_2O and the standard formation enthalpy of oxygen vacancies and electrons in CeO_2 were found to be equal to $\Delta_{ox,Cu_2O}H^0$ = (2.4 ± 0.4) eV and $\Delta_{red,CeO_2}H^0$ = (1.5 ± 0.3) eV, respectively. These findings are discussed in relation to the exceptional catalytic activity of copper-ceria for various oxidation-reduction reactions, focusing on the roles of both nano-dimensions and the influence of Cu on the redox properties of CeO_2.

1. Introduction

Enhanced macroscopic solubility of dopant elements has been reported in solids with high interface to volume ratios, such as materials with high specific grain boundary area (1), where excess solute is segregated at the grain boundaries (2-8). Similar observations have been made for surface segregation (8-10), of particular interest in catalysis. Here, the activity of catalysts depends on their surface chemistry, which can, at best, only be estimated from volume phase equilibrium data.

Copper-doped cerium dioxide, CeO_2, exhibits high catalytic activity for SO_2 reduction by CO (11) and for CO oxidation (12-14). In the water-gas shift reaction, Cu atoms in "$Ce_{0.8}Cu_{0.2}O_2$"are transformed to Cu_2O at 100 °C, then to metallic copper above 300°C (15). The catalytic activity of the mixed oxide is comparable to precious metal catalysts and is higher than that of unsupported pure copper or cerium dioxide, pointing to an important catalyst-support interaction (16), including reported interactions between Cu atoms and oxide ion vacancies in ceria (15). Most recently the rate of methanol production over a ceria/copper composite was found to be approximately 14 times faster than on the traditional Cu/ZnO catalyst, reportedly related to adsorption/ reaction sites with complementary chemical properties at the metal/oxide interface (17). This synergetic effect was explained by the stabilization of Cu^+ ions by ceria and enhanced active oxygen on ceria surfaces induced by the presence of copper, facilitating the formation of oxide ion vacancies (18).

While many factors have been suggested as supporting the exceptional catalytic activity of the Cu-ceria system, there have been no direct quantitative correlations regarding the concentration of key defect species in ceria, the modified thermodynamics e.g. change in reduction enthalpies and Cu segregation versus precipitation of Cu into a three dimensional phase.

Microstructural analysis of $Cu_{0.15}Ce_{0.85}O_{2-x}$ samples by X-ray diffraction (XRD) and transmission electron microscopy (TEM) revealed that copper oxide was highly dispersed on cerium oxide and that this dispersion was remarkably stable (19). Cupric oxide, CuO, only formed as a distinct phase during annealing at temperatures above 550 ºC at $pO_2 = 0.15$ bar; this coincided with grain growth of the cerium oxide matrix. In systems with positive enthalpy of mixing, the thermodynamic activity increases monotonically with solute concentration, until the

equilibrium solubility is reached and the solute precipitates as a new phase. One might thus ask whether the observed formation of CuO is a consequence of the thermal activation becoming sufficient for crystallization to occur (a kinetic effect), or the consequence of a loss of interfacial area, due to grain growth, inducing CuO to crystallize (a thermodynamic effect).

To our knowledge, no phase diagram of the Cu-Ce-O system has been established. In the related Cu-Zr-O system, no ternary compound and a very small solid solubility of copper in cubic ZrO_2 have been reported. Taking into account that Ce is an even larger cation than Zr, the solubility of copper in the CeO_2 fluorite lattice must be expected to be very low due to the large difference in ionic radii. Electron paramagnetic resonance studies (20) showed that CeO_2 containing 1% Cu exhibited surface segregation with an enrichment factor of 25, supporting the assumption of a rather low solubility of Cu in the CeO_2 matrix.

Given that the emf of an electrochemical cell depends on the thermodynamic activity of the components in the electrodes, the activity of copper oxides in nanostructured mixed copper-cerium oxide could be determined by potentiometric measurements (21). A suitable electrochemical cell, operating at 320ºC, was composed of a Cu-doped CeO_2 working electrode, copper(I) bromide, CuBr, as solid electrolyte (22, 23) and a Cu/Cu_2O or Cu_2O/CuO reference electrode. The measured activities of CuO and Cu_2O dispersed in nanostructured cerium oxide were consistent with an apparent macroscopic solubility, due to interfacial segregation of copper oxide on the nanostructured cerium oxide. With an average grain diameter of about 18 nm, a monolayer of Cu and O atoms was formed at the grain interfaces at a copper molar fraction $x_{Cu} \approx$ 0.1; the activity curve changed monotonically up to this value and could be represented by a modified Langmuir-MacLean equation (24). For higher molar fractions, crystallization of Cu_2O and a constant activity were observed, as expected for bi-phase equilibrium. The measured free energy of segregation, $\Delta_{seg}G \approx 0.4$ eV, is related to the strain energy resulting from differences of the radii of the host Ce^{4+} and Cu ions (9, 25); the observed value is matching with an ionic radius between those reported for Cu^+ and Cu^{2+} (26).

Although the general thermodynamic behavior has been investigated, many questions remain relating to the driving force for interface segregation of copper oxides in ceria and its implications, for example, for the electrical and catalytic properties of the Cu-modified ceria. Presumably, the type of crystalline oxide formed, CuO or Cu_2O, depends on the temperature and oxygen partial pressure in the gas phase, while the amount of Cu coming out of solution depends

as well on the particle size. Measurements of the electrical properties of such nano-scale oxides are an excellent means for monitoring the impact of oxygen partial pressure, temperature and/or grain coarsening on secondary phase formation. This is particularly the case here, since the equilibrium electrical properties of single crystal and nano-sized ceria are well known (10, 27-32), rendering ceria solid solutions as model materials for this kind of investigation.

In this study of the evolution of Cu-doped CeO_2 nanopowders during annealing at intermediate temperatures (≤500 ºC), the electrical properties and the mechanical compaction are simultaneously determined by *in-situ* impedance spectroscopy and dilatometry. The following questions are addressed: 1) How does the oxidation state of copper vary as a function of pO_2 at given isotherms and are these changes reversible? 2) Is the formation of oxide monolayers related to a densification of the cerium oxide particles? 3) What are the temperature and oxygen partial pressure dependences of the electrical properties of the nano-composites?

Another feature of this study is that properties of nanosized oxide particles are investigated prior to their sintering into dense ceramics. The use of very small nanoparticles, furthermore, allows one to focus on surface effects, which is of particular importance in heterogeneous catalysis.

2. Experimental

Cu-doped CeO_2 nanopowder appears as black, slightly agglomerated particles. The Cu-containing ceria nanoparticles were prepared by the urea gelation co-precipitation (UGC) method, which produces more homogeneous mixed oxides with finer particle sizes than conventional coprecipitation (33). The UGC method involves the following steps: dissolution of urea, $(NH_4)_2Ce(NO_3)_6$ and $Cu(NO_3)_2.3H_2O$ in required amounts (8 mol% Cu) in deionized water, heating the solution to boiling, leading to precipitation. The precipitate is then washed in deionized water, dried in an oven at 100 °C, crushed in an agate mortar and calcined at 650 °C for 4h. A detailed description may be found in Ref. 40. Powder X-Ray diffraction (XRD) was performed for phase analysis and average particle size determination (34) prior to and following heat treatment. A PANalytical X'Pert PRO instrument was used with CuKα radiation (λ = 0.1504 nm) and 0.014 °/s scan rate.

The experimental arrangement, allowing simultaneous dilatometry and electrochemical impedance spectroscopy (EIS) measurements, was presented previously (35). In short, the lightly compacted nanopowder is contained in a quartz crucible with a sputtered Pt film at the base; a spring-loaded quartz rod retains the nanopowder, maintains the electrical contact to the second 3 mm diameter sputtered Pt electrode, and allows monitoring of the sample expansion or contraction.

Mixtures of O_2/N_2 and $H_2/H_2O/N_2$ were used to fix the oxygen partial pressure within the sample chamber; it was measured above 500°C by an oxygen sensor inside the sample chamber or calculated from thermodynamic relations, ranging from 1 to ~10^{-40} bar. The gas ratios and flow rates were adjusted by mass flow controllers.

Electrochemical impedance spectroscopy (EIS) measurements were performed using a Novocontrol Alpha-A Impedance Analyzer (Hundsangen, Germany) over a frequency range of 0.1 Hz to 1 MHz in a temperature range between 50 °C to 500°C.

3. Results

3.1. Nanoparticle structure and size

The as-received Cu-doped ceria nanopowders were found by powder XRD to solely contain the fluorite CeO_2 phase (Figure 1, black line). In spite of the black color of the powders, no trace of crystalline copper oxides, neither CuO (JCPDF 48-1548, Tenorite) nor Cu_2O (JCPDF 05-0667), was observed. However, the relative Bragg peak intensities are somewhat different from the JCPDS reference values, showing some preferred orientation. Furthermore, the peaks of the as-received samples are slightly shifted versus higher Bragg angles. Using line profile analysis and the Scherrer equation:

$$D = \frac{\lambda}{B\cos\theta} \qquad (1)$$

where B is the full peak width at half maximum (FWHM) in radians and θ the Bragg angle, an average crystallite size D = (4 ± 2) nm was determined. A Williamson-Hall analysis gave identical results. After the experiments, no crystalline copper oxides, copper metal or new phases could be detected (red line). The FWHM was significantly reduced, showing that some

crystallite growth took place; the average crystallite size remained low, however, at (10 ± 6) nm (Figure 1). The relatively small size increase may be related to the stabilization of ceria nano-crystallites by copper oxide segregation, as reported above.

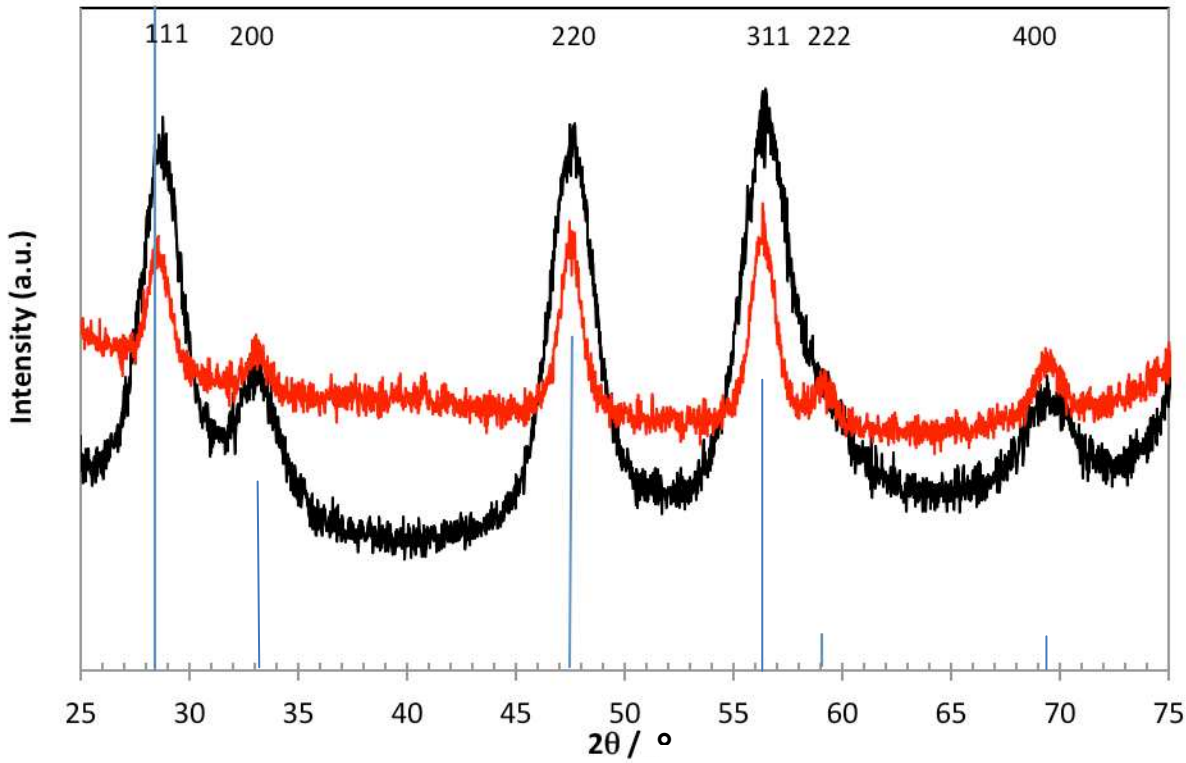

Figure 1. XRD patterns of Cu-doped CeO_2 nanopowder: as-received (black curve) and at the end of the experiment (red curve). The reference peaks of CeO_2 (JCPDS file nr. 00-004-0593) are superimposed as blue lines.

3.2.Dilatometry

Figure 2 shows typical dilatometric curves obtained during the initial heating of the Cu-doped nanopowder. As one can see in Figure 2a, very dramatic shrinkage is observed above 400ºC, so that this temperature was exceeded only for short times. Compaction by more than 3% was already observed up to 200ºC (Figure 2b).

a)

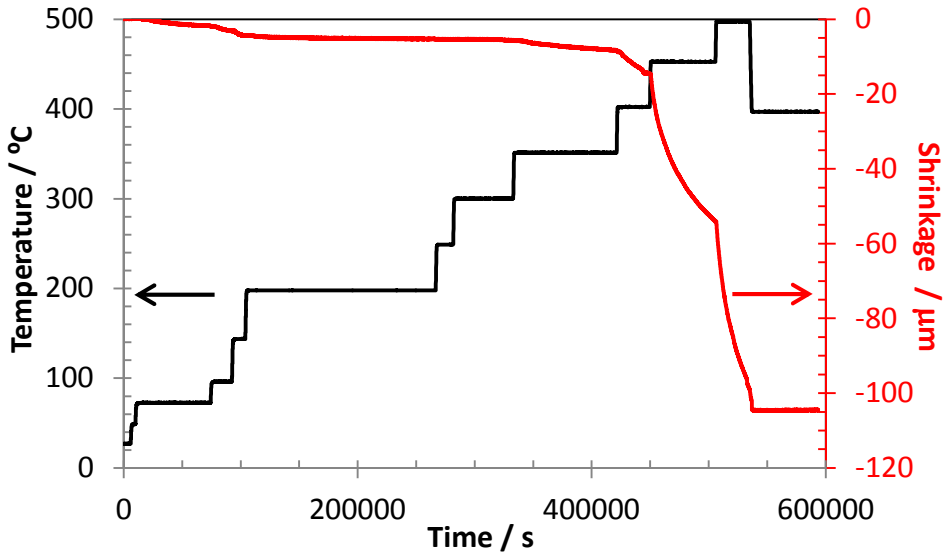

b)

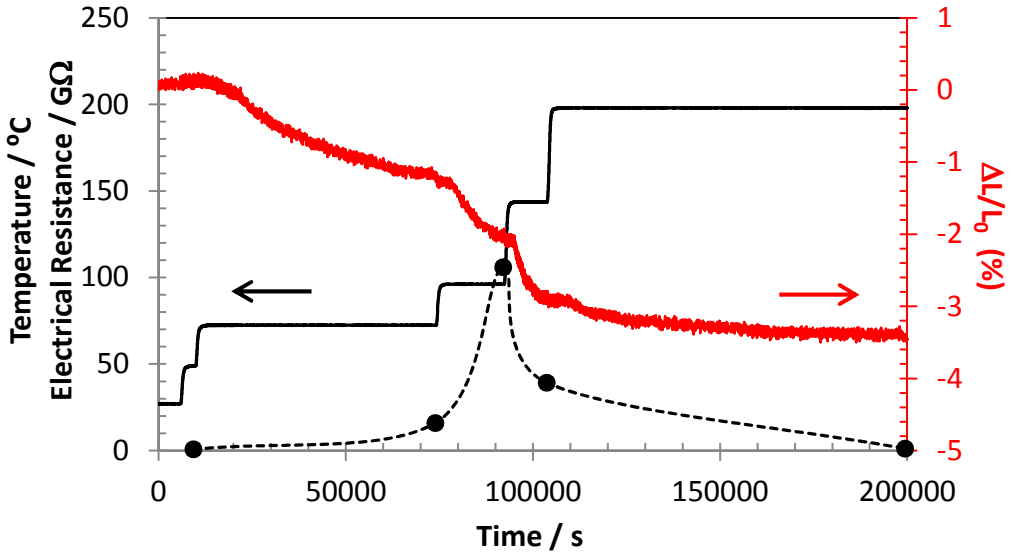

Figure 2.a) In-situ dilatometric curve of as-received Cu-doped CeO_2 powder. b) Zoom-in on the initial 200000 s of the previous figure. The electrical resistance, at various times, is also indicated (black dots, the dashed line is a guide to the eye).

The shrinkage is very slow and cannot be fitted by any reasonable time law, such as a square root time dependence. It is likely related instead to the thermally activated removal of surface water

molecules, as found in other nanocrystalline metal oxides (35, 36) (see also the discussion of electrical properties below).

The thermal expansion coefficient is estimated to be approximately 8 x10^{-5} K^{-1} between 250 and 350 ºC and 9 x 10^{-5} K^{-1} between 350 and 400ºC from the data in Figure 3a. These values are clearly larger than the ones reported for bulk ceria (~10^{-5} K^{-1} (37, 38)). Chemical expansion, due to the formation of oxide ion vacancies and Ce^{3+} ions under reducing conditions[44], should not play a major role, as the data in Figure 3a were obtained at high pO_2. Tentatively, this observation might be ascribed to the segregation of copper oxide at the grain or particle boundaries, leading to free volume between the ceria nanoparticles (see cartoon in Figure 4). On a subsequent cooling-heating cycle (Figure 3b), the variation is not fully reversible and hysteresis is observed. This can be ascribed to some irreversible compaction of the nano-powders.

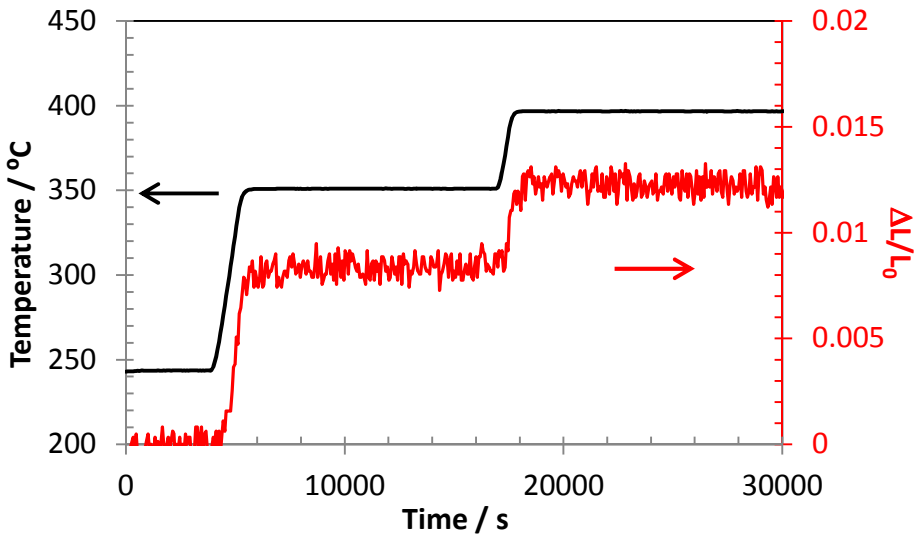

Figure 3a. Thermal expansion of Cu-doped CeO_2 powder in air.

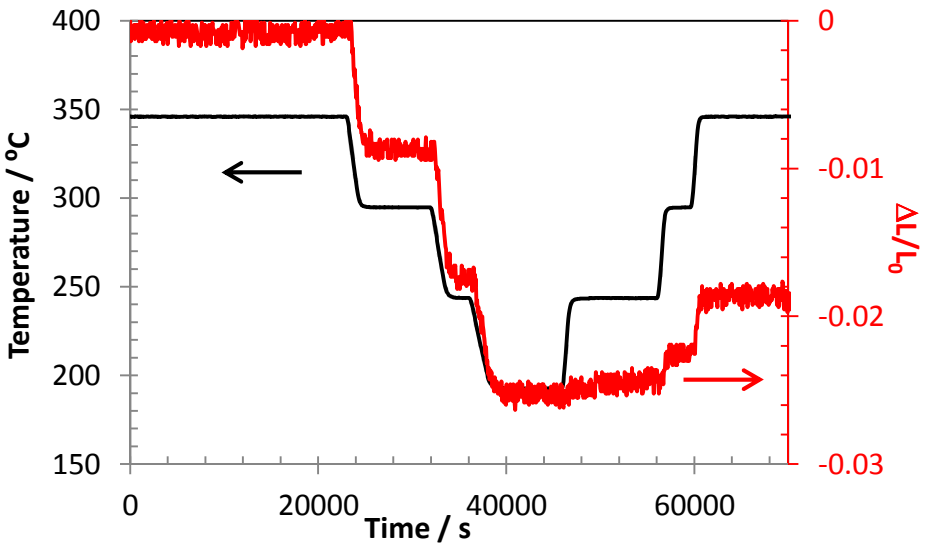

Figure 3b. Cooling-heating cycle of Cu-doped CeO_2 powder in air. A clear hysteresis is observed, probably related to irreversible compaction of the nanopowder.

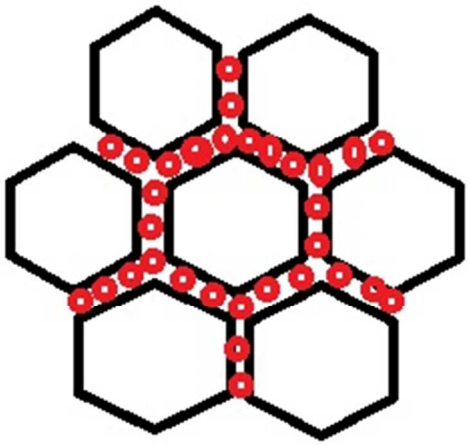

Figure 4. Schematic representation of nano-sized CeO_2 grains (black polygons) with segregated non-percolating layer of copper oxide (or copper, red circles). Some free volume is indicated inside the segregation layer.

Figure 5 shows the thermometric and dilatometric curves observed during the reduction of segregated copper oxide into metallic Cu at 450ºC in a 5% $H_2/H_2O/N_2$ mixture.

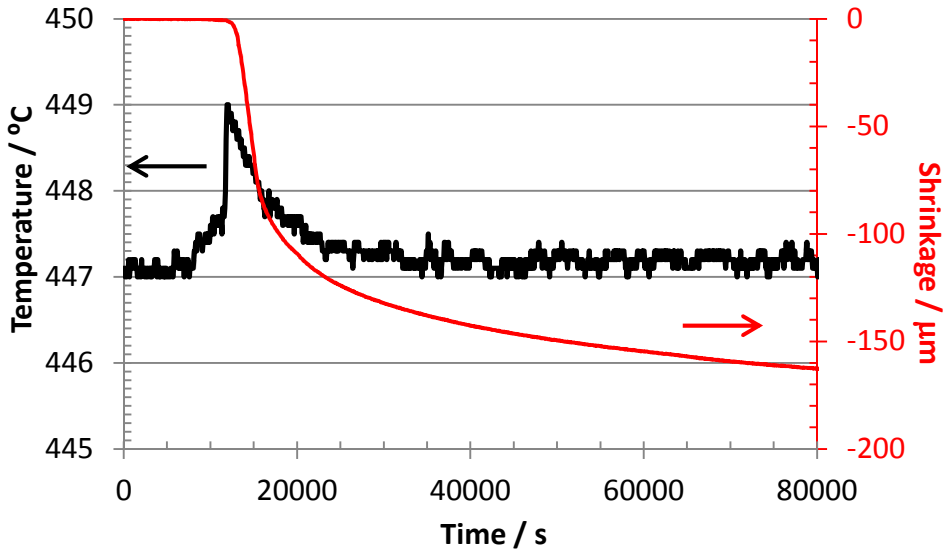

Figure 5. Dilatometric and thermometric curves during copper oxide reduction to metallic Cu under $pO_2 \approx 10^{-36}$ bar.

The reduction of Cu_2O in the presence of hydrogen gas

$$Cu_2O + H_2 \rightarrow 2\ Cu + H_2O \qquad (2)$$

is an exothermic reaction with a standard enthalpy of -73.2 kJ/mol (note the sample temperature rose by several degrees during introduction of the $H_2/H_2O/N_2$ mixture). The expected volume reduction can be calculated from the molar volumes of Cu (7.1 cm^3/mol) and Cu_2O (23.9 cm^3/mol). Qualitatively, the thermometric and dilatometric curves reflect the heat and volume change of this reaction, but the shrinkage can only be understood if some compaction of the CeO_2 is concurrently taking place. The re-oxidation of segregated copper into Cu_2O in air, clearly observed in the electrical measurements (see below), is not visible by dilatometry, even though several unsuccessful attempts were made to observe it.

3.3. Electrical properties

Figure 6 shows typical impedance spectra for Cu-doped CeO_2 measured in air at 350 °C before and after segregation of copper oxide. The spectra are characterized by a large nearly ideal semi-circle except for the lowest frequencies for which a second much smaller contribution appears.

The electrical properties were extracted from the spectra by fitting an equivalent circuit model, consisting of two parallel (resistor//constant phase element [CPE]) components in series, one representing the grain interior (large semicircle) and the other representing partially blocking particle-particle contacts (small semicircle). The conductance values are calculated from the low frequency intersection of the larger impedance arc with the real axis while the smaller contribution is not further considered. The sample conductance and capacitance (from about 10 to 300 pF) increase by about 30 times, following the segregation of the copper oxide.

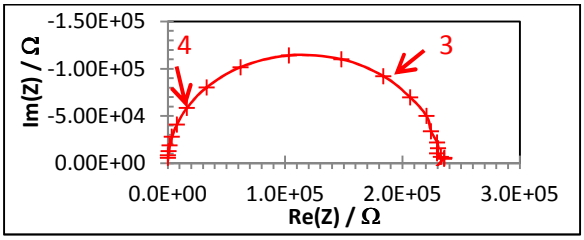

b)

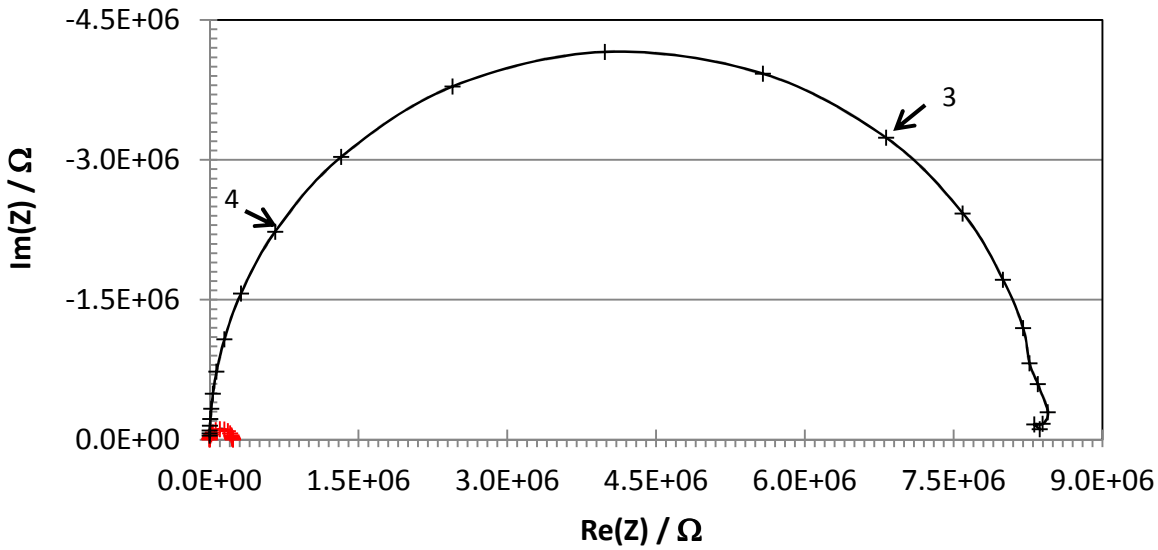

a)

Figure 6. Typical impedance plot of Cu-doped CeO_2 at 350ºC in air a) before segregation (black crosses) and b) after segregation of copper oxide (red crosses). Numbers alongside the curve indicate log (frequency) values at which representative data points were taken.

The electrical resistance of the as-received Cu-doped CeO_2 nanopowder below 200 ºC during the first heat treatment is shown in figure 2b: the initial resistance increase can be attributed to the removal of parasitic proton conduction by hydroxide groups and water at the ceria surface (35,

36, 39). This is consistent with the minimum in conductance observed for the first heating cycle at ~100ºC as shown in Figure 7. The conductance in the temperature range 50-100ºC follows an Arrhenius-type dependence (open dots) with an activation energy of about -1 eV, which is near the enthalpy of adsorption of water on nanocrystalline cerium dioxide for low surface coverage (40). One should mention that Maier and coworkers found a lower activation energy, -(0.3-0.4) eV, for proton conduction in ceria (39), which might correspond to larger water coverage, allowing for a Grotthuss-type conduction contribution. After this initial water removal, and upon further heating, the conductance plot at pO_2 = 1 bar (black dots in Figure 7) gives an average activation energy of (0.9 ±0.1) eV, which we suspect is related to the reduction enthalpy of nano-sized CeO_2 (see discussion below).

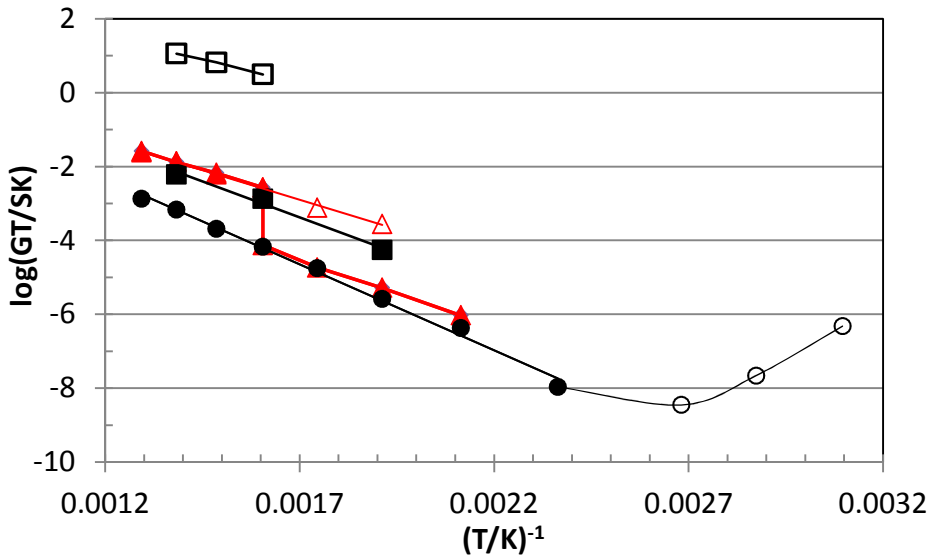

Figure 7. Arrhenius plots of conductance for pO_2 / bar = 1 (○ and ●), 0.2 (▲), 0.1 (△), ~10^{-30} (□). The conductance following re-oxidation under pO_2 = 0.2 bar is also indicated (■).

At pO_2 = 0.2 bar, an abrupt change of resistance is noticed at 350°C, where a very thin and more highly conducting copper oxide interfacial layer apparently percolates through the CeO_2 matrix; the dilatometric curve does not show any discontinuity at this point. While the formation of a conducting copper oxide interfacial layer was observed in several experiments in the temperature range of around 350°C, the absence of an exact transformation temperature indicates kinetic

limitations. The activation energy calculated from the data above percolation, reported in Figure 7 (open red triangles), is (0.6±0.1) eV.

If strongly reducing conditions are applied, i.e., 5% $H_2/H_2O/N_2$ gas mixture at 450ºC, the change in the impedance spectra (Figure 8) is even more spectacular, with the conductance increasing by nearly 3 orders of magnitude, suggesting the formation of metallic copper at the interfaces. However, the conductance data in Figure 7 (open squares), surprisingly, still exhibit a thermally activated behavior, with comparable activation energy prior to reduction, suggesting that the metallic copper layer is not fully percolating. This interpretation is consistent with the large capacitance increase, observed when copper oxide segregates, given the formation of space charge regions at the interfaces between the n-type ceria and p-type copper oxide.

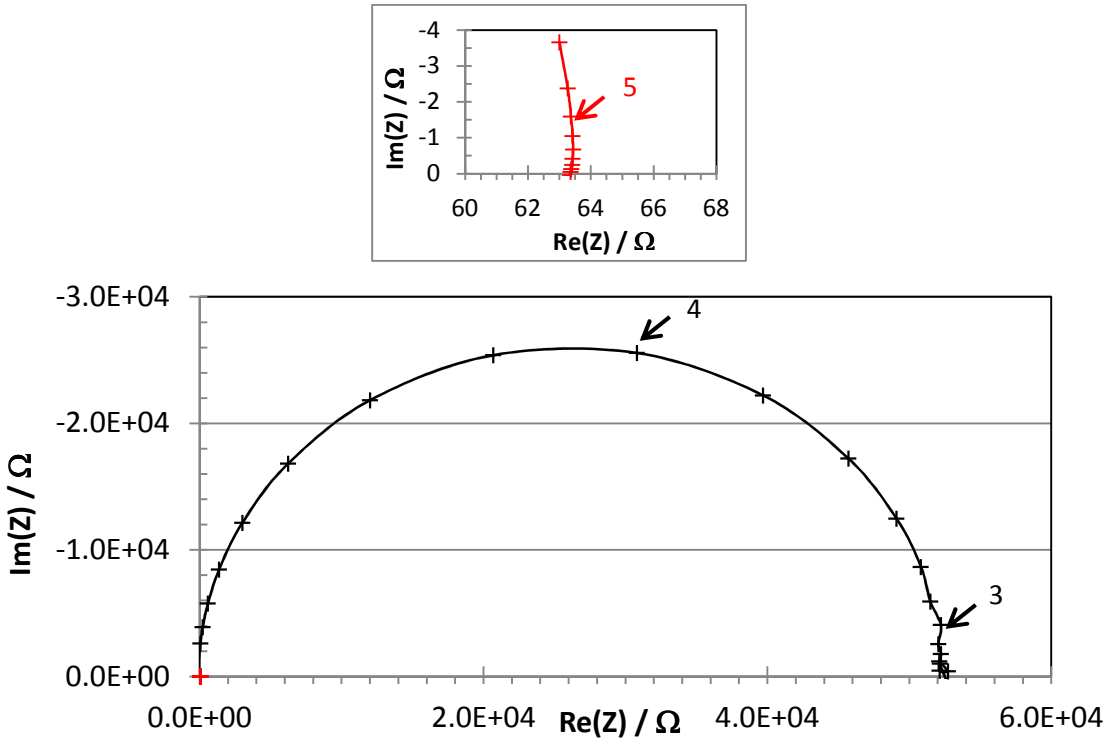

Figure 8. Impedance plots before (black crosses) and after the formation of metallic copper (red crosses) at 450ºC in a 5% $H_2/H_2O/N_2$ gas mixture.

4. Discussion

4.1. Review of defect and transport properties of the oxides of cerium and copper

CeO_2 is known to become oxygen-deficient under reducing conditions at elevated temperatures by the formation of oxide ion vacancies ($V_O^{\bullet\bullet}$) and electrons, which can be written according to the Kröger-Vink nomenclature as (41, 42):

$$O_O \rightleftharpoons \frac{1}{2}O_2 + V_O^{\bullet\bullet} + 2e' \quad (3)$$

The corresponding mass action relation is given by:

$$[V_O^{\bullet\bullet}]n^2 pO_2^{1/2} = K_{red,CeO_2}(T) = K^0_{red,CeO_2} \exp\left(-\frac{\Delta_{red,CeO_2}H^0}{kT}\right) \quad (4)$$

The square bracket signifies concentration, n is the electron density, and $K_{red,CeO_2}(T)$ is the reduction equilibrium constant. The pre-exponential factor K^0_{red,CeO_2} contains the standard entropy and $\Delta_{red,CeO_2}H^0$ is the standard enthalpy of reduction associated with reaction 1. k is Boltzmann's constant and T the absolute temperature.

The condition of bulk charge neutrality can be approximated by the equation:

$$2[V_O^{\bullet\bullet}] = n + [A'_{Ce}] \quad (5)$$

with A'_{Ce} representing ionized acceptor dopants, commonly found as background impurities in ceria. Under highly reducing conditions, following Eq. 1, the electroneutrality condition can be approximated by:

$$2[V_O^{\bullet\bullet}] \approx n \quad (6)$$

Solving for the oxide ion vacancy and electron concentrations under these conditions by substitution of Eq. 6 into Eq. 4, one obtains:

$$2[V_O^{\bullet\bullet}] = n = (2K_{red,CeO_2})^{1/2} pO_2^{-1/6} \quad (7)$$

while for more oxidizing conditions, $[A'_{Ce}]$ dominates the right hand side of Eq. 5 leading to

$$n = \left(\frac{2K_{red,CeO_2}}{[A'_{Ce}]}\right)^{1/2} pO_2^{-1/4} \quad (8)$$

By examining the pO_2 dependence of the electron density, one can establish the controlling neutrality condition and then relate the measured activation energy to either $\frac{\Delta_{red,CeO_2}H^0}{3}$ or $\frac{\Delta_{red,CeO_2}H^0}{2}$ depending on whether the oxygen vacancies are predominantly compensated by electrons or by acceptor impurities. In a previous study by this group, the electrical conductivity of nominally undoped CeO_2 nanoparticles followed a $pO_2^{-1/6}$ dependence, pointing to electron compensation (43). Given that electrons in ceria move via a thermally activated small polaron hopping mechanism (44), one must take this into account in interpreting the measured activation energy of conduction. Thus, since $\sigma = ne\mu_e$ where μ_e is the electron mobility, the activation energy for conduction is given by:

$$\Delta_\sigma H = \frac{\Delta_{red,CeO_2}H^0}{3} + \Delta_\mu H \qquad (9)$$

where $\Delta_\mu H$ is the electron hopping energy, which for ceria is 0.4 eV (44). The measured $\Delta_\sigma H$ of the ceria particles, prior to percolation of the segregated boundary phases (black dots in Figure 6), is equal to (0.9 ± 0.1) eV. This value is similar to values reported for a variety of forms of nominally undoped nanocrystalline ceria including dense bulk (0.99 eV; 1.16 eV) (10), thin film (1.3 eV) (45) and powder (1.3 eV) (43). Substituting this value of $\Delta_\sigma H$ and the reported value for $\Delta_\mu H$ into Eq. 9 results in a value for $\Delta_{red,CeO_2}H^0$ of (1.5 ± 0.3) eV, about one third of the value for undoped coarsened ceria powder of ~40 nm particle size ((4.5 ± 0.4) eV (10)). This result can also be compared to the derived value for $\Delta_{red,CeO_2}H^0$ for undoped nano-ceria particles ((2.7 ± 0.4) eV) with a lower average diameter of 25 nm diameter, which also shows a considerably lower reduction enthalpy than that of the larger 40 nm particles. Generally, a lower reduction enthalpy can be associated with sufficiently small particle size (4 nm in this study) given the large enhancement in the number of oxide ions residing near the surface of these very small particles, where reduction is expected to be enhanced (46). Below, we consider, as well, the potential role of Cu in causing an additional decrease in the magnitude of the reduction enthalpy.

Several studies exist on cuprous oxide Cu_2O, finding it to be metal-deficient with the majority atomic defects attributed to neutral copper ion vacancies at high pO_2 (47-49). Haugsrud and

Norby (48) reported an expression for the Cu diffusivity in Cu_2O and deduced the enthalpy of formation of uncharged copper vacancies to be 60 kJ/mol, whereas the migration enthalpy was estimated to be 54 kJ/mol. Moore and Selikson (50) agreed on the prevailing defect, but found an activation energy for copper diffusion of 141 kJ/mol. Porat and Riess reported instead uncharged copper interstitials as majority point defects at low temperature and uncharged oxygen vacancies at high temperature (47, 51), but they also stated the formation enthalpy of neutral copper vacancies to be 60 kJ/mol.

The electronic majority defects at high oxygen partial pressures (pO_2) are electron holes formed by ionization of the neutral Cu vacancies acting as acceptor states. The formation of ionized copper ion vacancies $V_{Cu}^{'}$ and electron holes $h^{\bullet}$ can be written according to the following quasichemical reaction (41):

$$2Cu_{Cu} + \frac{1}{2}O_2 \rightleftharpoons 2V_{Cu}^{'} + 2h^{\bullet} + Cu_2O \qquad (10)$$

The corresponding mass action reaction reads:

$$[V_{Cu}^{'}]^2 \, p^2 \, pO_2^{-1/2} = K_{ox,Cu_2O}(T) = K_{ox,Cu_2O}^{0} \exp\left(\frac{-\Delta_{ox,Cu_2O}H^0}{kT}\right) \qquad (11)$$

Here p is the concentration of electron holes and $\Delta_{ox,Cu_2O}H^0$ the standard enthalpy of oxidation of cuprous oxide. Porat and Riess provide a value for $\Delta_{ox,Cu_2O}H^0$ which they estimate to be (1.8 ± 0.2) eV. For sufficiently high pO_2, the simplified electro-neutrality equation can be written as:

$$[V_{Cu}^{'}] \approx p \qquad (12)$$

Solving for the copper vacancy and electron hole concentrations under these conditions by substituting Eq. 12 into Eq. 11, one obtains:

$$[V_{Cu}^{'}] = p = (K_{ox,Cu_2O})^{1/4} \, pO_2^{1/8} \qquad (13)$$

The complete temperature and oxygen partial pressure dependence of the electron hole conductivity of Cu_2O can finally be written:

$$\sigma = pe\mu_h = (K_{ox}^{0})^{1/4} \, e\mu_h \, pO_2^{1/8} \exp\left(-\frac{\Delta_{ox,Cu_2O}H^0}{4kT}\right) \qquad (14)$$

In this equation, μ_h is the electron hole mobility (which is not thermally activated) with the other terms defined above. The electrical conductivity isotherms reported in the literature show partial

pressure exponents ranging from +1/3 to +1/8, depending on the temperature range. The larger exponents were attributed to various defect complexes, such as those between ionized and non-ionized copper ion vacancies (49). In conclusion, Cu_2O is a *p*-type semiconductor with a small ionic transference number ($t(Cu^+) = 5.10^{-4}$ (52)) and an electron hole conductivity which depends on the oxygen activity (48, 53, 54).

For purposes of later discussion, we also include the intrinsic Schottky disorder reaction of Cu_2O given by

$$nil \rightleftharpoons 2V_{Cu}^{'} + V_O^{\bullet\bullet} \qquad (15)$$

with the equilibrium constant given by:

$$\left[V_{Cu}^{'}\right]^2\left[V_O^{\bullet\bullet}\right] = K_{Sch,Cu_2O}(T) = K_s^0 \exp\left(\frac{-\Delta_{Sch,Cu_2O}H^\circ}{kT}\right) \qquad (16)$$

where $\Delta_{Sch,Cu_2O}H^\circ$ is the standard Schottky formation enthalpy. We also note that Equations 3 and 4 apply equally to Cu_2O under sufficiently reducing conditions, with the entropy and enthalpy values substituted appropriate to the material (e.g. CeO_2 vs Cu_2O) under consideration.

Data on the non-stoichiometry of cupric oxide CuO are not available and transport studies are incomplete. The conductivity of CuO is apparently not dependent on the oxygen activity, but due to significant intrinsic electron-hole pair formation, and can be described by:

$$nil \rightleftharpoons e' + h^\bullet \qquad (17)$$

with the equilibrium constant given by:

$$np = K_i(T) = K_i^0 \exp\left(-\frac{E_g}{kT}\right) \qquad (18)$$

where E_g is the band gap energy. If intrinsic electronic conductivity is assumed and one neglects any temperature dependence of the electron hole mobility, then the conductance activation energy of 1.01 eV, in the temperature range of 600-950ºC, would correspond to a band gap of about 2.0 eV (53). Obviously, Equations 17 and 18 apply as well to Cu_2O and CeO_2 with the appropriate band gaps and pre-exponential terms (product of the effective density of states in the conduction and valence bands) substituted.

4.2. Electrical conductivity of nanocomposite oxides

For interpreting the electrical data of our nano-composite system, we assume that following segregation, nanostructured "CuO_x" forms an interfacial layer of 0.5 nm thickness, in accordance with the Fisher grain boundary model (55).

The AC electrical properties of two-phase mixtures can be described, using the complex conductivity σ_i*, defined as (56):

$$\sigma_i^* = \sigma_i + j\omega\varepsilon_i \qquad (19)$$

j is the imaginary unit and ω the angular frequency (in rad/s). σ_i is the dc conductivity and ε_i the dielectric permittivity of phase i. We have previously simulated and discussed the impedance spectra of composite solids (57-59). In our case, an interfacial layer (copper oxide or metallic copper) is assumed between the CeO_2 grains. The segregated layer being much more conductive than the CeO_2 grain interior, conduction along the interfaces is assumed to be dominant and one can consider a simplified network where the complex total conductivity, σ_t*, is given by (56):

$$\sigma_t^* = \sigma_{gi}^* + \frac{2}{3} x_{\text{int}} \sigma_{\text{int}}^* \approx \frac{2}{3} x_{\text{int}} \sigma_{\text{int}}^* \qquad (20)$$

In this equation, σ_{gi}^*, σ_{int}^* and x_{int} are, respectively, the complex conductivity of the grain interior (corresponding to nano-sized CeO_{2-x}), the complex interfacial conductivity (corresponding to the assumed copper oxide or metallic copper interfacial layer) and the volume fraction of the interfacial region, which can be estimated from the CeO_2 grain size D and the interfacial layer width d:

$$x_{\text{int}} \approx \frac{2D^2 d}{D^3} = \frac{2d}{D} \qquad (21)$$

If we take as grain diameter D = 4 nm using Scherrer's equation, we obtain x_{int} = 0.25. The sample should show only one arc in the impedance spectrum (56, 58, 59), if perpendicular interfaces are non-blocking. The conductance is additive for parallel circuits, so that it is determined by the larger interfacial contribution (56). One single arc is observed in the typical impedance plots represented in Figures 7 and 8, as predicted when boundaries are non-blocking.

The capacitance of as-received Cu-doped CeO_2 is between 11 and 12 pF between 200 and 500ºC. Using a relative dielectric constant of 25 for ceria in this temperature domain, these values are consistent with a powder thickness of approximately 0.15 mm. Following what is believed to be the segregation of a percolating copper oxide layer at 350 ºC (cf. Figure 6), one notices a reproducibly large increase in capacitance to values between 300 and 330 pF, consistent with the

formation of internal p-n junctions between the p-type Cu_2O and the n-type CeO_2, as noted above.

On subsequent heating-cooling cycles, the impedance data are consistent with the behavior of Cu_2O instead of CuO, although the latter is reported to be the equilibrium phase in the investigated temperature and pO_2 range. This suggests that the interaction between ceria and copper oxide at the boundaries stabilizes Cu_2O, due to the higher surface energy of CuO, which plays an important role for such highly divided solids. The surprising stability of Cu_2O nanocrystals has been reported previously (60).

The oxygen partial pressure dependence of conductivity after percolation of the thin Cu_2O layer at pO_2 between 1 bar and 0.05 bar is represented in Figure 9. A characteristic exponent +(0.12±0.02) is observed, near the one reported for Cu_2O (+1/8, see equation 14). This suggests that the observed activation energy E_A = (0.6 ± 0.1) eV (violet data points in Figure 6) should be interpreted in terms of the standard enthalpy of oxidation of Cu_2O, corresponding to Eq. 14. Given that Porat and Riess report that the hole mobility is not thermally activated (51), one obtains from Equation 14 that $\Delta_{ox,Cu_2O}H^0 = 4*E_A$ = (2.4 ± 0.4) eV. This is considerably larger than the value of (1.8 ± 0.2) eV obtained by Porat and Riess for bulk Cu_2O (51).

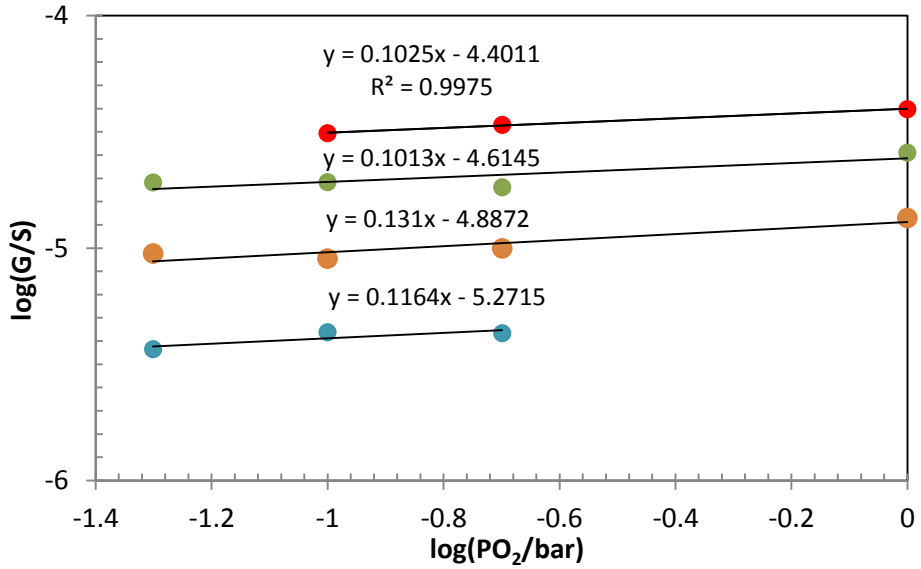

Figure 9. Conductance isotherms as function of pO_2 of Cu-doped CeO_2 nanopowder at 500 (●), 450 (●), 400 (●) and 350 ºC (●). The average exponent is +1/8.

Interestingly, equilibrium in nano-sized powder specimens appears to be attained at temperatures considerably below those required for pressed ceramic disks, as data at 350 ºC can be described by expressions based on the assumption of the attainment of equilibrium. Perhaps this is not surprising given the very thin nature of the Cu_2O layer ($d \leq 0.5$ nm) and the highly porous nature of the pressed nanoparticles.

At this point, it is interesting to examine how the observations made in this study may provide insight into the observations of the exceptional catalytic activity of copper-ceria for various oxidation-reduction reactions. In this regard, the very recent publication by Colussi et al. (18) is helpful, since in it the authors summarize key features noted about the CuO_x/CeO_2 catalyst system. These include enhanced oxygen mobility in ceria upon transition metal doping (61, 62), facilitation of the formation of oxygen vacancies in ceria by Cu (15), the stabilization of Cu^+ species by ceria (16, 63) and the mutual reduction of copper oxide and ceria (64).

First, let us examine the suggested facilitation of the formation of oxygen vacancies on ceria. We did indeed find that the reduction enthalpy for Cu-doped CeO_2 nanoparticles ($\Delta_{red,CeO_2}H^0 =$ (1.5 ± 0.3) eV) was considerably reduced compared to that obtained by us earlier for nominally undoped CeO_2 nanoparticles ($\Delta_{red,CeO_2}H^0 =$ (2.7 ± 0.4) eV). While the undoped particles were larger than the Cu-doped particles (25 vs 4 nm), we do not believe that this alone was the source of the large decrease in the effective reduction enthalpy. We suspect instead that the segregated Cu ions on the ceria particle surface, which initially remain in solid solution with ceria, serve to reduce the effective reduction enthalpy of ceria. This, we believe, is due to two key factors: first, the relative ease of reduction of Cu^{2+} to Cu^+ compared to that of Ce^{4+} to Ce^{3+} and, second, the considerably smaller radius of the Cu ion relative to the Ce ion. It is instructive to compare the Shannon radii (65) of the relative ionization states of Cu and Ce. One observes that the Cu ion radii are roughly 60-80% of those of the Ce ions ($r(_{Cu}{}^{+})$ = 0.77Å; $r(_{Cu}{}^{2+})$ = 0.73 Å in 6-fold coordination[1]) as compared to those of Ce ($r(_{Ce}{}^{3+})$ = 1.196 Å; $r(_{Ce}{}^{4+})$ = 0.97 Å in 8-fold coordination).

The authors recently demonstrated the role of *redox-facile* elements in facilitating the reduction of ceria in their study of Pr doped ceria (66, 67). There is was demonstrated that the addition of

[1]Cu is normally not 8-fold coordinated by oxygen

Pr, which readily reduces from Pr^{4+} to Pr^{3+}, even under oxidizing conditions, results in an effective decrease in the reduction enthalpy of ceria from 4.76 to 1.9 eV (66, 67).

The addition of smaller radius dopants to ceria, even if they are not multivalent (e.g. Zr) have also been demonstrated to induce ceria to reduce more readily. In recent studies by the authors on $Ce_{0.8}Zr_{0.2}O_{2-\delta}$, they found that the reduction enthalpy of ceria was reduced to (2.87 ± 0.06) eV (68, 69). Here, the decrease in reduction energy is correlated with the desire of the smaller element to surround itself with fewer oxygens and thereby have an oxygen coordination lower than 8, as required by the fluorite structure. The fact that Cu is considerably smaller than Ce, and that it is a redox active element under oxidizing conditions, is thus entirely consistent with the large effective drop in $\Delta_{red,CeO_2}H^0$ observed in this study.

Next we turn to the reported observation that Cu^+ is stabilized by ceria and that ceria enhances the reduction of copper oxide (16, 63). What we find in this study is that the enthalpy of oxidation of Cu_2O, in contact with ceria, increases by about a third compared to pure Cu_2O, i.e. $\Delta_{ox,Cu_2O}H^0(Cu_2O/CeO_2)$ = (2.4 ± 0.4) eV versus $\Delta_{ox,Cu_2O}H^0(Cu_2O)$ = (1.8 ± 0.2) eV. What we would like to know instead is what would be the magnitude of $\Delta_{red,CeO_2}H^0$. One can easily show that $\Delta_{red,Cu_2O}H^0$ and $\Delta_{ox,Cu_2O}H^0$ are not independent of each other. Indeed it is straightforward that by combining Equations 4, 11, 16 and 18 (all appropriate to Cu_2O – see comments above) that

$$K_{Sch}(T)K_i(T)^2 = K_{ox}(T)K_{red}(T) \qquad (22)$$

This in turn implies that

$$\Delta_{Sch}H^\circ + 2E_g = \Delta_{Ox,Cu_2O}H^0 + \Delta_{red,Cu_2O}H^0 \qquad (23)$$

Thus, assuming the intrinsic formation energies for electron-hole and Schottky defects do not change significantly for Cu_2O on ceria, then any increase in the oxidation enthalpy must result in a corresponding decrease in the reduction enthalpy. As $\Delta_{ox,Cu_2O}H^0$ was found to increase by approximately 0.6 eV in Cu_2O on ceria compared to isolated Cu_2O, one can according to Eq. 23 assume that $\Delta_{red,Cu_2O}H^0$ has decreased by the same amount. This indeed would be consistent with our present observations, i.e. an expected decrease in the reduction enthalpy of Cu_2O on ceria compared to Cu_2O alone.

5. Conclusions

The segregation of copper oxide or copper interface layers on Cu-doped $CeO_2$was studied by electrical and dilatometric measurements. The electrical properties of the nanoparticle array, extracted from impedance spectroscopy studies, point to proton conduction at low temperatures, with a transition to n-type electronic conductivity of CeO_2 at higher temperatures. After segregation of percolating interfacial layers, induced by exposure to reducing atmosphere, the electrical properties become dominated by p-type Cu_2O at intermediate pO_2 and metallic copper at low pO_2. The temperature and pO_2 dependent electrical properties of both the Cu_2O shell and the underlying ceria core were examined in light of defect chemical models. Based on these models, the formation enthalpy of copper vacancies and holes in Cu_2O and the formation enthalpy of oxygen vacancies and electrons in CeO_2 were found to be equal to $\Delta_{ox,Cu_2O}H^0$ = (2.4 ± 0.4) eV and $\Delta_{red,CeO_2}H^0$ = (1.5 ± 0.3) eV, respectively.

These findings were discussed in relation to the exceptional catalytic activity of copper-ceria for various oxidation-reduction reactions, focusing on the roles of both nano-dimensions and the influence of Cu on the redox properties of CeO_2.

Specifically, we found that the highly reduced effective enthalpy of reduction of the Cu-doped CeO_2 nanoparticles, compared to undoped CeO_2 nanoparticles helps explain many of the key features reported for Cu-doped ceria catalysts including the facilitation in the formation of oxygen vacancies on ceria by Cu, and enhanced oxygen mobility (which in turn relies on the existence of a high vacancy concentration). Likewise, the increased enthalpy for oxidation of Cu_2O on ceria compared to isolated Cu_2O, derived from the electrical measurements, was shown to be consistent with the enhanced reducibility of Cu_2O on Cu doped ceria catalysts. Furthermore, this study was able to provide thermodynamic and kinetic data that can be used in support of future efforts to model the catalytic activity of Cu-doped ceria catalysts. More broadly, this study confirms the utility of combined *in-situ* dilatometry and impedance spectroscopy for the study of complex nanostructured and nanocomposite materials.

Acknowledgments

The authors acknowledge the US-Department of Energy - Basic Energy Sciences, Grant No. DE-SC0002633 for financial support. This work made use of the MRSEC Shared Experimental

Facilities at MIT, supported by the National Science Foundation under award number DMR-0819762 including the assistance of Dr. Scott Speakman with the XRD analysis.

P. K. wishes to thank H. L. T. for the kind hospitality during his sabbatical at the Massachusetts Institute of Technology and H.L.T likewise wishes to thank P.K. for his kind hospitality during a week-long visit to Aix-Marseille University during the preparation of this manuscript.

6. References

1. Gleiter H. Nanostructured Materials: Basic Concepts and Microstructure. Acta mater. 2000;**48**:1-29.
2. Bouchet R, Weibel A, Knauth P, Mountjoy G, Chadwick AV. EXAFS study of dopant segregation (Zn, Nb) in nanocrystalline anatase (TiO_2). Chemistry of Materials. 2003;15(26):4996-5002.
3. Ikeda JAS, Chiang Y-M. Space Charge Segregation in Titanium Dioxide. J Am Ceram Soc. 1993;**76**:2437-46.
4. Ikeda JAS, Chiang YM, Garratt-Reed AJ, Vander Sande JB. Space-charge segregation at grain-boundaries in titanium-dioxide 2. Model experiments. Journal of the American Ceramic Society. 1993;76(10):2447-59.
5. Knauth P, Chadwick AV, Lippens PE, Auer G. EXAFS Study of Dopant Ions with Different Charges in Nanocrystalline Anatase: Evidence for Space-Charge Segregation of Acceptor Ions. Chemphyschem. 2009;10(8):1238-46.
6. Weibel A, Bouchet R, Knauth P. Electrical properties and defect chemistry of anatase (TiO_2). Solid State Ionics. 2006;177(3-4):229-36.
7. Lippens PE, Chadwick AV, Weibel A, Bouchet R, Knauth P. Structure and chemical bonding in Zr-doped anatase TiO_2 nanocrystals. Journal of Physical Chemistry C. 2008;112(1):43-7.
8. Porat O, Tuller HL, Lavik EB, Chiang YM, editors. Coulometric titration studies of nonstoichiometric nanocrystalline ceria. Symposium on Nanophase and Nanocomposite Materials II, at the 1996 MRS Fall Meeting; 1996 Dec 02-05; Boston, MA. Warrendale: Materials Research Society; 1997.
9. Wynblatt P, Ku RC. Surface-energy and solute strain-energy effects in surface segregation. Surface Science. 1977;65(2):511-31.
10. Chiang YM, Lavik EB, Kosacki I, Tuller HL, Ying JY. Nonstoichiometry and electrical conductivity of nanocrystalline CeO_{2-x}. Journal of Electroceramics. 1997;1(1):7-14.
11. Tschope A, Liu W, Flytzani-Stephanopoulos M, Ying JY. Redox activity of nonstoichiometric cerium oxide-based nanocrystalline catalysts. Journal of Catalysis. 1995;157(1):42-50.
12. Tschope A, Ying JY, Tuller HL. Catalytic redox activity and electrical conductivity of nanocrystalline non-stoichiometric cerium oxide. Sensors and Actuators B-Chemical. 1996;31(1-2):111-4.
13. Sedmak G, Hocevar S, Levec J. Kinetics of selective CO oxidation in excess of H_2 over the nanostructured $Cu_{0.1}Ce_{0.9}O_{2-y}$ catalyst. Journal of Catalysis. 2003;213(2):135-50.

14. Yang F, Graciani J, Evans J, Liu P, Hrbek J, Sanz JF, et al. CO Oxidation on Inverse CeO_x/Cu(111) Catalysts: High Catalytic Activity and Ceria-Promoted Dissociation of O_2. Journal of the American Chemical Society. 2011;133(10):3444-51.
15. Wang XQ, Rodriguez JA, Hanson JC, Gamarra D, Martinez-Arias A, Fernandez-Garcia M. In situ studies of the active sites for the water gas shift reaction over Cu-CeO2 catalysts: Complex interaction between metallic copper and oxygen vacancies of ceria. Journal of Physical Chemistry B. 2006;110(1):428-34.
16. Kundakovic L, Flytzani-Stephanopoulos M. Reduction characteristics of copper oxide in cerium and zirconium oxide systems. Applied Catalysis a-General. 1998;171(1):13-29.
17. Graciani J, Mudiyanselage K, Xu F, Baber AE, Evans J, Senanayake SD, et al. Highly active copper-ceria and copper-ceria-titania catalysts for methanol synthesis from CO_2. Science. 2014;345(6196):546-50.
18. Colussi S, Amoroso F, Katta L, Llorca J, Trovarelli A. The Effect of Ceria on the Dynamics of CuO-Cu_2O Redox Transformation: CuO-Cu_2O Hysteresis on Ceria. Catalysis Letters. 2014;144(6):1023-30.
19. Tschope A, Ying JY, Chiang YM. Processing and structural evolution of nanocrystalline Cu-CeO_{2-x} catalysts. Materials Science and Engineering a-Structural Materials Properties Microstructure and Processing. 1995;204(1-2):267-71.
20. Aboukais A, Bennani A, Aissi CF, Wrobel G, Guelton M, Vedrine JC. Highly resolved electron-paramagnetic resonance-spectrum of copper(ii) ion-pairs in Cu-Ce oxide. Journal of the Chemical Society-Faraday Transactions. 1992;88(4):615-20.
21. Knauth P, Schwitzgebel G, Tschope A, Villain S. Emf measurements on nanocrystalline copper-doped ceria. Journal of Solid State Chemistry. 1998;140(2):295-9.
22. Villain S, Desvals MA, Clugnet G, Knauth P. Study of polycrystalline CuBr and the interface Cu/CuBr by impedance spectroscopy. Solid State Ionics. 1996;83(3-4):191-8.
23. Tortet L, Knauth P, Tuller HL. Electrical conductivity of polycrystalline copper(I) bromide at low temperature (160-300 K). Solid State Ionics. 2002;146(3-4):423-7.
24. Guggenheim EA. Thermodynamics. Amsterdam, New York: North Holland; 1949.
25. Chiang YM, Lavik EB, Blom DA. Defect thermodynamics and electrical properties of nanocrystalline oxides: Pure and doped CeO_2. Nanostructured Materials. 1997;9(1-8):633-42.
26. Marcus Y. Ionic-radii in aqueous-solutions. Chemical Reviews. 1988;88(8):1475-98.
27. Tuller HL, Nowick AS. Doped ceria as a solid oxide electrolyte. Journal of the Electrochemical Society. 1975;122(2):255-9.
28. Nowick AS, Vaysleyb AV, Kuskovshy I. Universal dielectric response of variously doped CeO_2 ionically conducting ceramics. Physical Review B. 1998;58(13):8398-406.
29. Hwang JH, Mason TO. Defect chemistry and transport properties of nanocrystalline cerium oxide. Zeitschrift fur Phys Chemie. 1998;207:21-38.
30. Kim S, Maier J. On the conductivity mechanism of nanocrystalline ceria. Journal of the Electrochemical Society. 2002;149(10):J73-J83.
31. Knauth P. Ionic and electronic conduction in nanostructured solids: Concepts and concerns, consensus and controversies. Solid State Ionics. 2006;177(26-32):2495-502.
32. Lai W, Haile SM. Impedance spectroscopy as a tool for chemical and electrochemical analysis of mixed conductors: A case study of ceria. Journal of the American Ceramic Society. 2005;88(11):2979-97.

33. Qi XM, Flytzani-Stephanopoulos M. Activity and stability of Cu-CeO_2 catalysts in high-temperature water-gas shift for fuel-cell applications. Industrial & Engineering Chemistry Research. 2004;43(12):3055-62.
34. Weibel A, Bouchet R, Boulc'h F, Knauth P. The big problem of small particles: A comparison of methods for determination of particle size in nanocrystalline anatase powders. Chemistry of Materials. 2005;17(9):2378-85.
35. Engel J, Bishop SR, Vayssieres L, Tuller HL. In Situ Electrical Characterization of Anatase TiO_2 Quantum Dots. Advanced Functional Materials. 2014;24(31):4952-8.
36. Maglia F, Tredici IG, Spinolo G, Anselmi-Tamburini U. Low temperature proton conduction in bulk nanometric TiO2 prepared by high-pressure field assisted sintering. Journal of Materials Research. 2012;27(15):1975-81.
37. Kuru Y, Bishop SR, Kim JJ, Yildiz B, Tuller HL. Chemomechanical properties and microstructural stability of nanocrystalline Pr-doped ceria: An in situ X-ray diffraction investigation. Solid State Ionics. 2011;193(1):1-4.
38. Kossoy A, Frenkel AI, Feldman Y, Wachtel E, Milner A, Lubomirsky I. The origin of elastic anomalies in thin films of oxygen deficient ceria, CeO_{2-x}. Solid State Ionics. 2010;181(33-34):1473-7.
39. Shirpour M, Gregori G, Merkle R, Maier J. On the proton conductivity in pure and gadolinium doped nanocrystalline cerium oxide. Physical Chemistry Chemical Physics. 2011;13(3):937-40.
40. Hayun S, Shvareva TY, Navrotsky A. Nanoceria - Energetics of Surfaces, Interfaces and Water Adsorption. Journal of the American Ceramic Society. 2011;94(11):3992-9.
41. Kroger FA, Vink HJ. Relations between the concentrations of imperfections in crystalline solids. Solid State Physics-Advances in Research and Applications. 1956;3:307-435.
42. Kröger FA. The Chemistry of Imperfect Crystals. 2nd ed. Amsterdam: North-Holland; 1974.
43. Knauth P, Engel J, Bishop SR, Tuller HL. Study of compaction and sintering of nanosized oxide powders by in situ electrical measurements and dilatometry: Nano CeO_2—case study. Journal of Electroceramics. 2014:1-9.
44. Tuller HL, Nowick AS. Small polaron electron-transport in reduced ceo_2 single-crystals. Journal of Physics and Chemistry of Solids. 1977;38(8):859-67.
45. Litzelman SJ, Tuller HL. Measurement of mixed conductivity in thin films with microstructured Hebb-Wagner blocking electrodes. Solid State Ionics. 2009;180(20-22):1190-7.
46. Sayle TXT, Parker SC, Catlow CRA. Surface oxygen vacancy formation on ceo_2 and its role in the oxidation of carbon-monoxide. Journal of the Chemical Society-Chemical Communications. 1992(14):977-8.
47. Porat O, Riess I. Defect chemistry of $Cu_{2-y}O$ at elevated temperatures. Part I: Non-stoichiometry, phase width and dominant point defects. Solid State Ionics. 1994;74(3–4):229-38.
48. Haugsrud R, Norby T. Determination of thermodynamics and kinetics of point defects in Cu2O using the Rosenburg method. Journal of the Electrochemical Society. 1999;146(3):999-1004.
49. Peterson NL, Wiley CL. Diffusion and point-defects in Cu_2O. Journal of Physics and Chemistry of Solids. 1984;45(3):281-94.
50. Moore WJ, Selikson B. The diffusion of copper in cuprous oxide. Journal of Chemical Physics. 1951;19(12):1539-43.

51. Porat O, Riess I. Defect chemistry of $cu_{2-y}o$ at elevated-temperatures 2. electrical conductivity, thermoelectric power and charged point defects. Solid State Ionics. 1995;81(1-2):29-41.
52. Timm H, Janek J. On the Soret effect in binary nonstoichiometric oxides - kinetic demixing of cuprite in a temperature gradient. Solid State Ionics. 2005;176(11-12):1131-43.
53. Park JH, Natesan K. Oxidation of copper and electronic transport in copper oxides. Oxidation of Metals. 1993;39(5-6):411-35.
54. Scanlon DO, Morgan BJ, Watson GW, Walsh A. Acceptor Levels in p-Type Cu_2O: Rationalizing Theory and Experiment. Physical Review Letters. 2009;103(9):4.
55. Fisher JC. Calculation of diffusion penetration curves for surface and grain boundary diffusion. Journal of Applied Physics. 1951;22(1):74-7.
56. MacDonald JR. *Impedance Spectroscopy: Emphasizing Solid Materials and Systems*: Wiley; 1987.
57. Laugier JM, Raymond L, Albinet G, Knauth P. Numerical modelling of impedance spectra of ionic conductor-insulator core-shell composites. Modelling and Simulation in Materials Science and Engineering. 2011;19(6).
58. Bouchet R, Knauth P, Laugier JM. Theoretical analysis of IS of polycrystalline materials with blocking or conducting grain boundaries: From microcrystals to nanocrystals. Journal of the Electrochemical Society. 2003;150(7):E348-E54.
59. Bouchet R, Knauth P, Laugier JM. Theoretical analysis of the impedance spectra of electroceramics - Part 2: isotropic grain boundaries. Journal of Electroceramics. 2006;16(3):229-38.
60. Yin M, Wu CK, Lou YB, Burda C, Koberstein JT, Zhu YM, et al. Copper oxide nanocrystals. Journal of the American Chemical Society. 2005;127(26):9506-11.
61. Kim DK, Stowe K, Muller F, Maier WF. Mechanistic study of the unusual catalytic properties of a new Ni-Ce mixed oxide for the CO_2 reforming of methane. Journal of Catalysis. 2007;247(1):101-11.
62. Li GF, Wang QY, Zhao B, Zhou RX. Modification of $Ce_{0.67}Zr_{0.33}O_2$ mixed oxides by coprecipitated/impregnated Co: Effect on the surface and catalytic behavior of Pd only three-way catalyst. Journal of Molecular Catalysis a-Chemical. 2010;326(1-2):69-74.
63. Liu W, Flytzani-Stephanopoulos M. Transition metal-promoted oxidation catalysis by fluorite oxides: A study of CO oxidation over Cu-CeO_2. Chemical Engineering Journal. 1996;64(2):283-94.
64. Martinez-Arias A, Hungria AB, Fernandez-Garcia M, Conesa JC, Munuera G. Interfacial redox processes under CO/O_2 in a nanoceria-supported copper oxide catalyst. Journal of Physical Chemistry B. 2004;108(46):17983-91.
65. Shannon RD. Revised effective ionic-radii and systematic studies of interatomic distances in halides and chalcogenides. Acta Crystallographica Section A. 1976;32(SEP1):751-67.
66. Tuller HL, Bishop SR. Point Defects in Oxides: Tailoring Materials Through Defect Engineering. In: Clarke DR, Fratzl P, editors. Annual Review of Materials Research, Vol 41. Annual Review of Materials Research. 41. Palo Alto: Annual Reviews; 2011. p. 369-98.
67. Bishop SR, Stefanik TS, Tuller HL. Electrical conductivity and defect equilibria of $Pr_{0.1}Ce_{0.9}O_{2-delta}$. Physical Chemistry Chemical Physics. 2011;13(21):10165-73.

68. Kuhn M, Bishop SR, Rupp JLM, Tuller HL. Structural characterization and oxygen nonstoichiometry of ceria-zirconia ($Ce_{1-x}Zr_xO_{2-\delta}$) solid solutions. Acta Materialia. 2013;61(11):4277-88.
69. Chen D, Cao Y, Weng D, Tuller HL. Defect and Transport Model of Ceria–Zirconia Solid Solutions: $Ce_{0.8}Zr_{0.2}O_{2-\delta}$—An Electrical Conductivity Study. Chemistry of Materials. 2014;26(17):5143-50.